arXiv:1907.04034v2 [physics.comp-ph] 18 Feb 2020

An improved non-reflecting outlet boundary condition for weakly-compressible SPH

Pawan Negi[a,*], Prabhu Ramachandran[a], Asmelash Haftu[a]

[a]*Department of Aerospace Engineering, Indian Institute of Technology Bombay, Powai, Mumbai 400076*

Abstract

Implementation of an outlet boundary condition is challenging in the context of the weakly-compressible Smoothed Particle Hydrodynamics method. We perform a systematic numerical study of several of the available techniques for the outlet boundary condition. We propose a new hybrid approach that combines a characteristics-based method with a simpler frozen-particle (do-nothing) technique to accurately satisfy the outlet boundary condition in the context of wind-tunnel-like simulations. In addition, we suggest some improvements to the do-nothing approach. We introduce a new suite of test problems that make it possible to compare these techniques carefully. We then simulate the flow past a backward-facing step and circular cylinder. The proposed method allows us to obtain accurate results with an order of magnitude less particles than those presented in recent research. We provide a completely open source implementation and a reproducible manuscript.

Keywords: SPH, inlet, outlet, boundary conditions, Entropically Damped Artificial Viscosity

1. Introduction

The Smoothed Particle Hydrodynamics (SPH) method was independently introduced by Gingold and Monaghan [1], and Lucy [2] for simulation of astrophysical problems. Ever since, many SPH schemes have been introduced

*Corresponding author

Email addresses: pawan.n@aero.iitb.ac.in (Pawan Negi), prabhu@aero.iitb.ac.in (Prabhu Ramachandran), asmelash.a@aero.iitb.ac.in (Asmelash Haftu)

to solve a variety of fluid flow and elastic-dynamics problems (see [3] for a review). Monaghan [4] introduced the weakly-compressible SPH (WCSPH) to deal with incompressible fluids like water. An equation of state is introduced to relate the pressure to the density. There are two common problems with the WCSPH schemes. The first is the presence of particle disorder which reduces the accuracy of the scheme and the second is the presence of large pressure oscillations due to the stiff equation of state. Particle disorder can be ameliorated by the use of the Transport Velocity Formulation (TVF) [5, 6] or by using particle shifting [7, 8]. The pressure oscillations can be reduced by using a density smoothing [9], or by use of the δ-SPH formulation [10]. In the present work, we have used the Entropically Damped Artificial Compressibility SPH (EDAC SPH) [11] method that introduces a pressure evolution equation that damps any pressure oscillations. In addition to the WCSPH schemes discussed above, there are also a family of truly Incompressible SPH schemes [12, 13, 14] (ISPH). These schemes solve for a pressure-Poisson equation to find a suitable pressure distribution. These schemes require that a large, sparse system of linear equations be solved in order to compute the pressure.

Despite the many developments in the SPH method, there are some challenges in implementing accurate non-reflecting boundary conditions (NRBC) with the weakly-compressible formulations. One significant objective in implementing inlet and outlet boundary conditions is to let the pressure and velocity fluctuations pass out of the domain without affecting the internal particles. Lastiwka et al. [15] addressed this by extrapolating properties from within the fluid. To obtain first order consistency near the inlet and outlet, the reproducing kernel particle method given by Liu et al. [16] is used. Within the fluid, the corrected gradient given by Bonet and Lok [17] is used for accurate results. Any perturbations are passed out of the domain using characteristic variables and carefully chosen boundary conditions based on these characteristic variables.

Federico et al. [18] proposed freezing the properties of the fluid particles in the outlet. The outlet particles are advected with the frozen velocity. Marrone et al. [19] utilized the approach suggested by Federico et al. [18] and Lastiwka et al. [15] to simulate flows around bluff-bodies for a wide range of Reynolds numbers. Molteni et al. [20] proposes using a sponge layer in order to absorb waves coming from the domain in order to implement a non-reflective boundary and tested it on water waves inside a tank. In a method suggested by Khorasanizade and Sousa [21], the fluid is divided into

multiple sections perpendicular to the flow and the values from these zones are used to impose natural boundary conditions (zero-gradients of properties) to the inlet/outlet.

Recently, Alvarado-Rodríguez et al. [22] modified the NRBCs proposed by [23] for SPH. Tafuni et al. [24] proposes the use of ghost (or buffer) particles for inlet/outlet particles and use the higher order interpolation scheme of Liu and Liu [25] to extrapolate the property using a Taylor series expansion. Their approach allows them to treat the outlet and inlet buffer particles in the same way. Wang et al. [26] use the characteristic wave propagation velocity and perform Lagrange interpolation in the time domain to correctly implement NRBCs to simulate an under water blast in a small domain.

In the context of ISPH schemes, Hosseini and Feng [27] suggested a rotational pressure correction scheme in order to extrapolate pressure to the inlet or outlet and thereby impose natural boundary conditions. At the outlet, the last layer of fluid is copied up to a sufficient distance to ensure kernel support for the fluid particles. Pahar and Dhar [28] satisfy a divergence-free condition for the inlet and outlet by solving a pressure-Poisson equation along with the fluid particles. Monteleone et al. [29] investigated a novel approach in which only pressure boundary conditions were prescribed and velocity profiles are allowed to change according to it.

In the present work we focus on weakly-compressible schemes. It is clear that the method proposed by Lastiwka et al. [15] is ideal when one wishes to extrapolate properties from the fluid. This is most useful for inlets where one needs to extrapolate the pressure from the fluid into the inlet and prescribe the inlet velocity alone. However, for outlets, it is not clear which one of these methods is ideal for bluff body simulations. We find that there are a few important considerations that are not fully discussed in any of the earlier studies. Specifically, many realistic flows involving an outlet will have large vortices leaving the domain. These vortices involve both a pressure and velocity gradient. It is important that any outlet boundary condition not destroy these structures as doing so would affect the vortices upstream. These are typically handled by simply increasing the domain but this may not be needed if the outlet is carefully implemented. WCSPH schemes constantly generate pressure waves. These may be severe if the bodies are oscillating and this would introduce additional pressure waves which should be propagated out of the domain without vitiating any physical gradients like those due to vortices.

Efficiently testing an SPH outlet implementation in the context of the

above issues is critical. Doing so using a flow past cylinder benchmark is inefficient. We propose a suite of simple and efficient test problems that allow us to systematically investigate the boundary conditions. The benchmarks are the simple one-dimensional benchmark proposed by Lastiwka et al. [15], a two-dimensional wave, a free-vortex advecting with a mean flow, and a ramp inlet.

We implement the following boundary conditions and test them with the above benchmark problems and bring out the relative merits of each. The methods we implement are,

- a simple do-nothing boundary condition [21, 22] where the particle properties are frozen. We propose an improvement to this method .
- extrapolating the fluid properties to the outlet as proposed by Tafuni et al. [24] using a higher order interpolation.
- propagate the properties of the fluid into the outlet using the method of characteristic (MOC) Lastiwka et al. [15].
- a new hybrid approach that combines the do-nothing and MOC methods.

Based on our careful study, we see that all the existing methods have some difficulties. The hybrid method uses the best features of the available methods and performs much better with our test problems. The proposed modification to the traditional do-nothing also produces fairly good results and is very easy to implement. We finally apply these to the flow past a backward-facing step and a cylinder for Reynolds numbers in the range 20-200. We present the results in the entire computational domain showing the effectiveness of our implementation. The new boundary conditions allow us to obtain reasonable results with an order of magnitude fewer particles than previous results.

We use the open source PySPH [30, 31] framework for our simulations. Furthermore, in the interest of reproducible research, every figure presented in the results section of this manuscript is automated [32] and the source code is made available at `https://gitlab.com/pypr/inlet_outlet`. In the next section, we describe the SPH scheme we employ in some detail. Section 3, discusses the different techniques used to implement the outlet boundary conditions. Section 4 introduces the new test problems and compares the different boundary condition implementations.

2. The SPH method

In the present work, the EDAC (Entropically Damped Artificially Compressible) SPH scheme [11] is used to simulate incompressible fluid flow. The EDAC scheme uses a pressure evolution equation that is similar to the continuity equation but also contains a pressure damping term which reduces oscillations. The basic equations are the momentum equation,

$$\frac{d\mathbf{u}}{dt} = -\frac{1}{\rho}\nabla p + \nu\nabla^2\mathbf{u}, \tag{1}$$

where $\mathbf{u}$ is the velocity of the fluid, p is the pressure, and ν is the kinematic viscosity of the fluid. The EDAC pressure equation is given as,

$$\frac{dp}{dt} = -\rho c_s^2 \operatorname{div}(\mathbf{u}) + \nu_{edac}\nabla^2 p, \tag{2}$$

where c_s is the speed of sound, and the second term in the right hand side is the damping term and the viscosity used there is chosen as,

$$\nu_{edac} = \frac{\alpha h c_s}{8}. \tag{3}$$

α is chosen as 0.5, h is the SPH kernel smoothing length which is discussed further below and c_s is chosen such that $c_s = 10\ u_{\max}$ where $u_{\max}$ is an estimated maximum speed in the flow.

The EDAC SPH formulation [11] comes in two flavors. As we are primarily solving problems without a free surface in this work, we use the EDAC TVF formulation which employs the Transport Velocity Formulation of [5] along with the EDAC equation for evolving pressure, equation (2). This formulation ensures that the particle distribution is uniform through the use of a background pressure.

Particle volume for a particle i is evaluated using m_i/ρ_i where ρ_i is evaluated using the summation density,

$$\rho_i = \sum_j m_j W_{ij}, \tag{4}$$

where $W_{ij} = W(|\mathbf{r_i} - \mathbf{r_j}|, h)$ is the kernel function chosen for the SPH discretization and h is the kernel radius parameter. The summation is over all

the neighbors of particle i. In this paper, the quintic spline kernel is used, which is given by,

$$W(q) = \begin{cases} \alpha_2 \left[(3-q)^5 - 6(2-q)^5 + 15(1-q)^5\right], & \text{for } 0 \leq q \leq 1, \\ \alpha_2 \left[(3-q)^5 - 6(2-q)^5\right], & \text{for } 1 < q \leq 2, \\ \alpha_2 \, (3-q)^5, & \text{for } 2 < q \leq 3, \\ 0, & \text{for } q > 3, \end{cases} \tag{5}$$

where $\alpha_2 = 7/(478\pi h^2)$ in two-dimensions, and $q = |\mathbf{r}|/h$.

The present work utilizes a number density based formulation as discussed in [11]. The resulting discretized momentum equation is as follows:

$$\frac{\tilde{d}\mathbf{u}_i}{dt} = \frac{1}{m_i} \sum_j \left(V_i^2 + V_j^2\right) \Bigg[-\tilde{p}_{ij} \nabla W_{ij} + \frac{1}{2}(\mathbf{A}_i + \mathbf{A}_j) \cdot \nabla W_{ij} + \tilde{\eta}_{ij} \frac{\mathbf{u}_{ij}}{(r_{ij}^2 + \eta h_{ij}^2)} \nabla W_{ij} \cdot \mathbf{r}_{ij} \Bigg] + \mathbf{g}_i, \tag{6}$$

where $\mathbf{A} = \rho \mathbf{u}(\tilde{\mathbf{u}} - \mathbf{u})$, $\tilde{\mathbf{u}}$ is the advection or transport velocity and $\frac{\tilde{d}}{dt}$ is the material derivative associated with this transport velocity. $\mathbf{r}_{ij} = \mathbf{r}_i - \mathbf{r}_j$, $\mathbf{u}_{ij} = \mathbf{u}_i - \mathbf{u}_j$, $h_{ij} = (h_i + h_j)/2$, $\eta = 0.01$, $V_i = \frac{1}{\sum_j W_{ij}}$, and $\tilde{\eta}_{ij} = \frac{2\eta_i \eta_j}{\eta_i + \eta_j}$, where $\eta_i = \rho_i \nu_i$. An average pressure is subtracted to reduce errors in the pressure gradient. The average pressure is found as,

$$p_{\text{avg},i} = \sum_{j=1}^{N_i} \frac{p_j}{N_i}, \tag{7}$$

where N_i are the number of neighbors for the particle i and includes both fluid and boundary neighbors. This average pressure is used to define $\tilde{p}_{ij}$ as,

$$\tilde{p}_{ij} = \frac{\rho_j (p_i - p_{avg,i}) + \rho_i (p_j - p_{avg,i})}{\rho_i + \rho_j}. \tag{8}$$

The EDAC pressure evolution equation (2) is discretized using a similar approach to the momentum equation as,

$$\frac{dp_i}{dt} = \sum_j \frac{m_j \rho_i}{\rho_j} c_s^2 \, \mathbf{u_{ij}} \cdot \nabla W_{ij} + \frac{(V_i^2 + V_j^2)}{m_i} \tilde{\eta}_{ij} \frac{p_{ij}}{(r_{ij}^2 + \eta h_{ij}^2)} \nabla W_{ij} \cdot \mathbf{r}_{ij}, \tag{9}$$

where $p_{ij} = p_i - p_j$.

The particles move using the transport velocity as,

$$\frac{d\mathbf{r}_i}{dt} = \tilde{\mathbf{u}}_i. \tag{10}$$

The transport velocity is obtained from the momentum velocity $\mathbf{u}$ at each time step using,

$$\tilde{\mathbf{u}}_i(t+\delta t) = \mathbf{u}_i(t) + \delta t \left(\frac{\tilde{d}\mathbf{u}_i}{dt} - \frac{p_b}{m_i} \sum_j \left(V_i^2 + V_j^2 \right) \nabla W_{ij} \right), \tag{11}$$

where p_b is the background pressure. We choose the timestep and other parameters as discussed in [11]. The solid wall boundary conditions are implemented as discussed in [33, 11] and use a layer of ghost particles inside the solid. The pressure and velocity of the fluid is suitably projected on the solid. While we have employed the EDAC SPH scheme in our computations, we could have employed any WCSPH-based scheme for the purposes of this study.

3. Boundary conditions

In this work we are interested in simulating incompressible flow and in all of our test problems we have a prescribed velocity at the inlet. In order for a fluid particle with support radius h to have full support, one requires outlet/inlet particles. Fig. 1, shows a schematic for the particles at the inlet, outlet, and fluid. The particle properties at the inlet and outlet are evaluated using those of the fluid. As described in the previous section, the EDAC SPH scheme employs a pressure evolution equation that is not directly related to the fluid density. We therefore extrapolate pressure from the fluid to the inlet using the mirroring technique as described in Section 3.2. At the outlet, one needs to determine values of both the velocity and pressure. In this paper, we first evaluate the different existing approaches for implementing outlets and propose improvements in order to simulate NRBCs. In the following subsections, we describe the methods that we implement.

3.1. Do-nothing

Jin and Braza [23] advect the outgoing waves that pass through the outlet without reflecting them back into the domain for a mesh-based method using

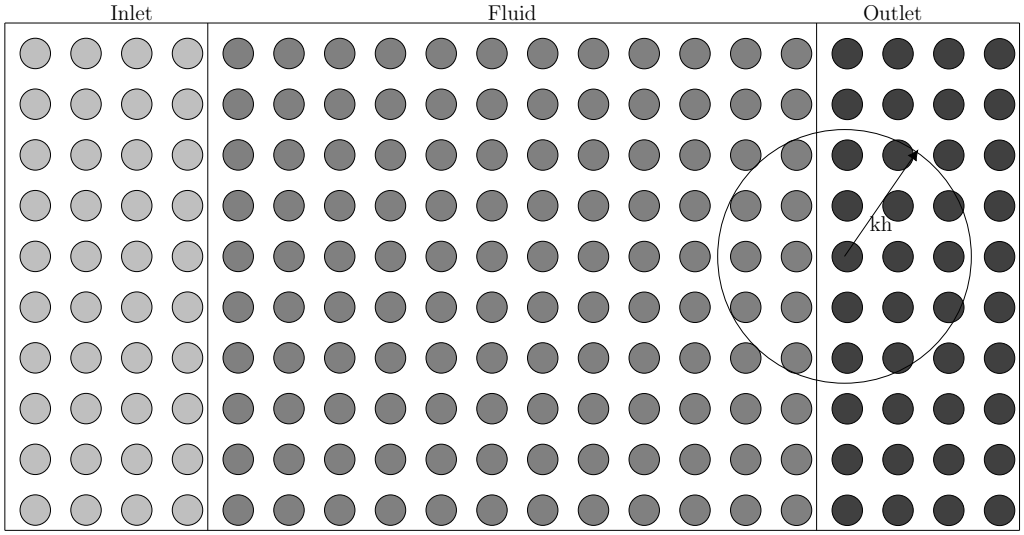


Figure 1: Sketch of the inlet, fluid, and outlet particle arrangement. The support for one outlet particle is also shown.

the MOC. The equation which can be used to propagate a wave through the outlet is given by

$$\frac{\partial \mathbf{u}}{\partial t} + u\frac{\partial \mathbf{u}}{\partial x} - \nu\frac{\partial^2 \mathbf{u}}{\partial y^2} = 0, \tag{12}$$

where $\mathbf{u}$ is the velocity vector, u is velocity component in x direction and ν is the kinematic viscosity. In this paper, the diffusion term has been dropped since the time for which outlet particles interact with the fluid particles is not long enough for diffusion. Thus the equation (12) reduces to

$$\frac{\partial \mathbf{u}}{\partial t} + u\frac{\partial \mathbf{u}}{\partial x} = 0. \tag{13}$$

Alvarado-Rodríguez et al. [22] proposes an SPH discretization of the equation (13), where the first term on the right-hand-side is considered as a material derivative and the velocity is integrated by taking the second term as acceleration. However, the equation (13) physically means one must advect the particles in the normal direction to the outlet while freezing all other properties like velocity and pressure. This is similar to the method proposed by Federico et al. [18]. In SPH form, at the outlet we can use

$$x_o^n = x_o^{n-1} + u_o^{n-1}\Delta t, \tag{14}$$

$$u_o^n = u_o^{n-1} \tag{15}$$

and

$$p_o^n = p_o^{n-1}, \tag{16}$$

where $*_o^n$ denotes the outlet properties at time n and x, u and p are the position, x-component of the velocity and pressure respectively.

3.1.1. Modified Do-nothing

We propose a subtle modification to the standard do-nothing method described in section 3.1. Unlike the standard do-nothing where the outlet moves with a velocity with which it left the fluid domain, we propose to extrapolate the velocity of the fluid to the advection velocity of the outlet particles. Thus the advection is given by

$$x_o^n = x_o^{n-1} + u_{ex}^n \Delta t, \tag{17}$$

where u_{ex}^n is the Shepard extrapolated fluid velocity at timestep n given as

$$u_{ex} = \frac{\sum_j u_j W_{ij}}{\sum_j W_{ij}}. \tag{18}$$

It must be noted that the advection velocities are only used to advect the particles and the actual velocity of the outlet particles remain the ones frozen when the fluid particle is converted to the outlet particle.

3.2. Mirroring

Tafuni et al. [24] employ a novel approach where the properties at the inlet/outlet are extrapolated using a Taylor series expansion about a mirrored particle at the fluid region. In the Fig. 2, we show the mirrored particles as circles with a dashed blue outline. The mirror particles are generated by reflecting inlet/outlet particles about the interface. Due to lack of kernel support at the interface, a higher order approximation given by Liu and Liu [25] is used to determine the property value at the mirrored particle.

In multiple dimensions, the first order Taylor series expansion for any property f of a particle about position $\mathbf{x}_k$ is

$$f(\mathbf{x}) = f_k + f_{k,\beta} \left(\mathbf{x} - \mathbf{x}_k \right). \tag{19}$$

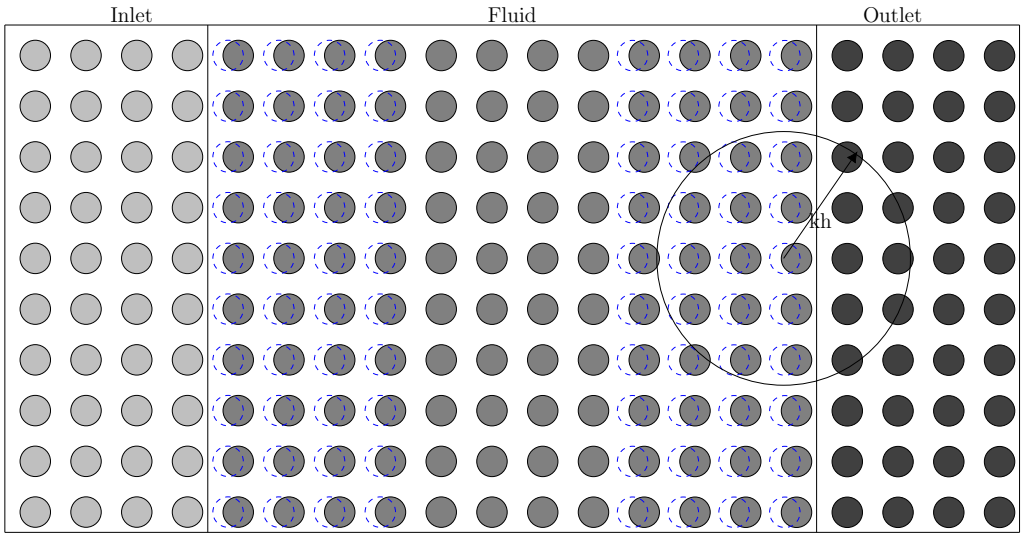


Figure 2: Inlet outlet particle arrangement. The dashed blue circles represent the reflected particles of the inlet and outlet about the interface.

Here $f_k = f(\mathbf{x}_k)$ and $f_{k,\beta}$ denotes the derivatives of the function and $\beta \in x, y, z$. Taking the inner product of the function with the SPH kernel $W_k(\mathbf{x}) = W(\mathbf{x} - \mathbf{x}_k)$ and it's derivative $W_{k,\beta}(\mathbf{x}) = W_\beta(\mathbf{x} - \mathbf{x}_k)$, we obtain

$$\int f(\mathbf{x}) W_k(\mathbf{x}) \mathrm{d}\mathbf{x} = f_k \int W_k(\mathbf{x}) \mathrm{d}\mathbf{x} + f_{k,\beta} \int (\mathbf{x} - \mathbf{x}_k) W_k(\mathbf{x}) \mathrm{d}\mathbf{x} \tag{20}$$

and

$$\int f(\mathbf{x}) W_{k,\beta}(\mathbf{x}) \mathrm{d}\mathbf{x} = f_k \int W_{k,\beta}(\mathbf{x}) \mathrm{d}\mathbf{x} + f_{k,\beta} \int (\mathbf{x} - \mathbf{x}_k) W_{k,\beta}(\mathbf{x}) \mathrm{d}\mathbf{x}. \tag{21}$$

Equations (20) and (21) can be written in matrix form using SPH approximation as

$$\begin{bmatrix} W_{kl}V_l & x_{lk}W_{kl}V_l & y_{lk}W_{kl}V_l & z_{lk}W_{kl}V_l \\ W_{kl,x}V_l & x_{lk}W_{kl,x}V_l & y_{lk}W_{kl,x}V_l & z_{lk}W_{kl,x}V_l \\ W_{kl,y}V_l & x_{lk}W_{kl,y}V_l & y_{lk}W_{kl,y}V_l & z_{lk}W_{kl,y}V_l \\ W_{kl,z}V_l & x_{lk}W_{kl,z}V_l & y_{lk}W_{kl,z}V_l & z_{lk}W_{kl,z}V_l \end{bmatrix} \begin{bmatrix} f_k \\ f_{k,x} \\ f_{k,y} \\ f_{k,z} \end{bmatrix} = \begin{bmatrix} f_l W_{kl} V_l \\ f_l W_{kl,x} V_l \\ f_l W_{kl,y} V_l \\ f_l W_{kl,z} V_l \end{bmatrix}, \tag{22}$$

where W_{kl} and $W_{kl,\beta} : \beta \in \{x, y, x\}$ are the kernel and it's derivative respectively, k denotes the destination index, l denotes the source particle index

and f is the property of interest, V_k is the volume of the k'th particle which in the present case is m/ρ, and $x_{kl} = x_k - x_l$. For brevity repeated indices l, are summed over. Note that the index k indicates the target particle which is fixed and not summed over. The above linear system is solved for each mirrored destination, which gives the property and it's derivative. After evaluating f and $f_{k,\beta}$, the values at inlet/outlet are evaluated using the Taylor series expansion given by

$$f_o = f_k + (\mathbf{r}_o - \mathbf{r}_k) \cdot \nabla f_k, \tag{23}$$

about the corresponding ghost particle position x_k. Tafuni et al. [24] extrapolate all the relevant properties using equation (23). In this paper, we have modified the equation for extrapolation to

$$f_o = f_k - (\mathbf{r}_o - \mathbf{r}_k) \cdot \nabla f_k. \tag{24}$$

in order to get zero gradient at the outlet interface. When we use the original form as written in [24], the test cases blow up.

3.3. Method of characteristics

This method has been proposed by Lastiwka et al. [15]. The basic idea is to resolve the perturbations from the mean flow in terms of the characteristics and then use the characteristic variables to propagate the appropriate values to the outlet or inlet. The scheme is itself based on the work of Giles [34] who proposes general NRBCs for the Euler equations.

The properties of fluid are rewritten in terms of the characteristic variables perpendicular to the outlet. In this process the appropriate boundary conditions may be applied. The following form of the characteristic variables is used,

$$\begin{aligned} J_1 &= -c_s^2(\rho - \rho_{ref}) + (p - p_{ref}) \\ J_2 &= \rho c_s(u - u_{ref}) + (p - p_{ref}) \\ J_3 &= -\rho c_s(u - u_{ref}) + (p - p_{ref}), \end{aligned} \tag{25}$$

where the $u_{ref}, p_{ref}, \rho_{ref}$ denote the reference quantities in the domain. We note that J_1, J_2, J_3 correspond to the quantities c_1, c_3, c_4 in the work of Giles [34]. The outflow boundary conditions basically require that J_1 and J_2 be determined from the interior and that J_3 be set to zero. The perturbations

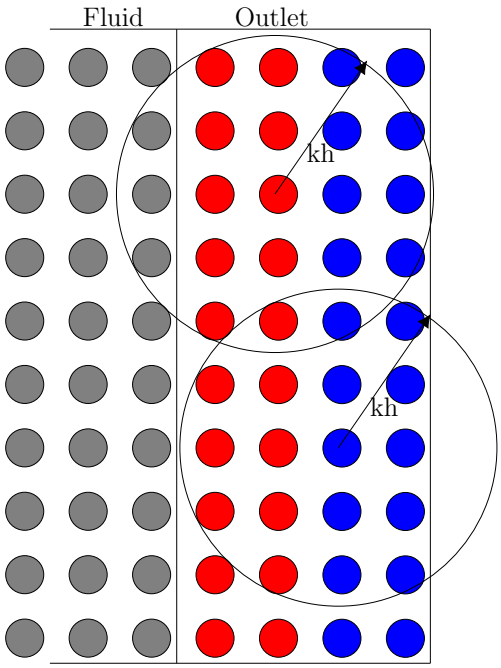


Figure 3: The outlet particles having fluid particles in their support radius are shown in red and without fluid particles in their support are in blue.

in the plane of the outlet pass through without any change, so the transverse components of the velocity are not changed by this scheme.

In our implementation we use a simple Shepard interpolation given by

$$f_i = \frac{\sum_j^N f_j W_{ij}}{\sum_j^N W_{ij}}, \tag{26}$$

where the i^{th} outlet particle is outside the fluid domain as shown in Fig. 1 and f is either J_1 or J_2. We use equation (26) to interpolate J_1, J_2 from the fluid to the outlet. Note that only some of the outlet particles are in the influence of the fluid. Fig. 3 shows a sketch of the outlet and fluid. As can be seen, the red particles are under the influence of the fluid but the blue particles are not. For the blue particles in the outlet which are outside the influence of the fluid particles i.e. $N = 0$, we find the J_1 and J_2 using the average of the values of red particles but at the previous timestep,

$$f_i^n = \frac{\sum_j^M f_j^{n-1}}{M}, \tag{27}$$

where M are the number of red particles which are in the support of the i^{th} blue particle. Given J_1, J_2, J_3 we can easily solve for the actual variables u, p, ρ using equation (25).

3.4. A new hybrid method

In this section, we describe a new method to implement outlet boundaries. At the outlet, essentially two kinds of fluctuations are encountered namely spatial variations which do not change rapidly in time and variations due to acoustic waves which travel with the speed of sound. The weakly compressible SPH schemes generate perturbations that travel with the prescribed speed of sound unlike with ISPH schemes which solve for a pressure-Poisson equation. In the case of a do-nothing type of outlet boundary as described earlier, the particle properties are frozen. As a result, when the acoustic wave arrives at the outlet, its velocity suddenly drops to the particle velocity in the outlet. This causes an increase in the pressure for particles that are near the outlet. In our proposed method, we devise a method to separate the fluid flow properties into acoustic and base flow properties.

A time averaged property of the flow is given by

$$f_{avg} = \frac{\sum_{n=1}^{N} f_n}{N}, \tag{28}$$

where f is the fluid property, N is the number of time steps used in the averaging. The value of N can be estimated by determining the number of time steps the acoustic wave takes to move from one particle to another given by

$$N = \frac{\Delta x}{\Delta t(u + c_s)}. \tag{29}$$

In all our cases $N \approx 4$, thus in order to have a sufficient time average we take $N = 6$ for all our test cases. Further, in order to detect the acoustic wave, the acoustic intensity is used as a parameter. The time averaged properties are not changed whenever the acoustic intensity of the flow is greater than the prescribed value. The acoustic intensity is given by $p^2/(2\rho c_s)$ [35]. The prescribed value of acoustic intensity can be determined using the inlet velocity, u_i and is given by

$$I = \frac{(\frac{1}{2}\rho u_i^2)^2}{2\rho c_s}. \tag{30}$$

The difference between the particle property and its time-average gives us the acoustic component. The time-averaged part is advected out of the domain using the do-nothing method. Since the acoustic wave travels with the speed of sound it should be propagated out with the same. We use the method of characteristics described in the previous section to propagate these acoustic perturbations into the outlet, where the reference values are the time-averages. In our implementation, we keep ρ_{ref} fixed.

When a particle moves from the fluid domain into the outlet, it retains its time average values. The acoustic properties are added to this using Shepard interpolation to the outlet zone as

$$f_o = f_{ac} + f_{avg}, \tag{31}$$

where f_{ac} is determined using the extrapolated J_2 as explained in section 3.3. Since the do-nothing condition is used at the outlet for the time-averaged values, the proposed method cannot simulate incoming flow near the outlet however it is suitable for wind tunnel type of flow where the flow always exits the outlet from one side. The particles in the outlet layer are advected using the velocity evaluated with equation (31) (assuming the outlet is perpendicular to the x-axis). The particles are not moved in the transverse direction. We note that the Shepard interpolation of the properties from the fluid will not always carry to all the particles in the outlet. These particles are advected with the average of the existing outlet advection velocity.

For all the inlet/outlet methods described here, inlet particles are added to the fluid particles whenever they cross the inlet-fluid interface. Similarly, at the outlet, fluid particles are removed and added to outlet whenever they cross the fluid-outlet interface. The particles are deleted once they leave the outlet region.

4. Results and discussion

In this section, we compare the different methods for the outlet boundary condition with a variety of test cases. Each of these cases only takes a small amount of computational effort and highlights specific issues. The new problems are all two-dimensional and this makes them relatively easy to implement. They include a one dimensional pulse (in a two-dimensional domain), a two-dimensional pulse, a two-dimensional vortex, and a ramp inlet condition in order to test the typical conditions that outlets encounter.

In order to obtain a solution representing an infinite domain for comparison, we simulate the flow in a very long domain. The properties of the fluid are measured at a probe placed inside the domain at a distance d from the inlet. The length of the domain, L is chosen to be $d + c_s t$, and t is the simulation time. We treat the fluid as inviscid and use a particle spacing of $\Delta x = 0.1$ unless stated otherwise in all our testcases. We use the results in the long domain as a reference and use this to compute the L_2 norm of the errors in the various properties using

$$e(f) = \left(\frac{\sum_n (f^n - f_l^n)^2}{\sum_n (f_l^n)^2} \right)^{1/2}, \tag{32}$$

where n represents the timestep, f^n is the property of interest at a particular timestep and f_l^n is the corresponding property in the long domain. Once these test cases are simulated we demonstrate the best of these methods for an impulsively started flow past a circular cylinder at different Reynolds numbers and a backward-facing step.

4.1. 1D Pressure bump

This test case was proposed by Lastiwka et al. [15]. In this testcase, the fluid domain is initialized with a pressure variation given by

$$p(x) = 1.0 - 0.2e^{\frac{-(x-0.5)^2}{0.001}}. \tag{33}$$

The pressure at inlet and outlet is initialized with $p = 1.0$. Velocity of the domain including inlet and outlet remain constant (=1m/s) for all times. The domain length is $1m$ and the pressure bump is at $x = 0.5m$. We use the artificial viscosity parameter, $\alpha = 0.1$ as mentioned in [15]. We simulated the testcase for all the types of outlet boundaries described in the section 3. In case of the MOC for all the test cases u_{ref}, p_{ref} and ρ_{ref} is taken as $1.0m/s$, 1.0 Pa and $1000kg/m^3$ respectively. In Fig. 4, we compare the pressure along the centerline of the domain at different times for all the methods. It can be seen that mirroring technique results in a significant drop in pressure towards the end. The modified do-nothing increases the pressure in the domain by a small amount. All other cases, match well with the MOC and with the long domain.

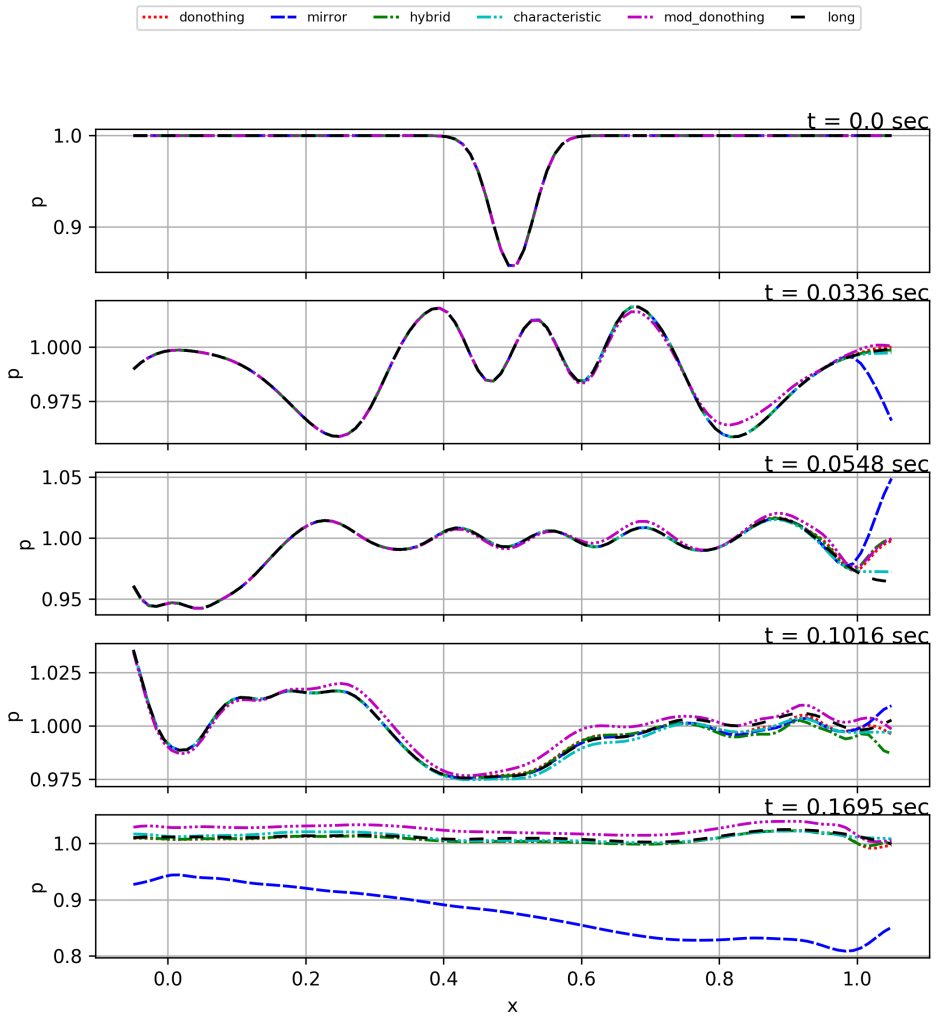


Figure 4: Pressure plot at various times for the different methods. The solid line denotes the solution with the long domain.

4.2. 2D pulse

This benchmark tests the non-reflectivity for a two-dimensional disturbance. A 2D domain is considered, consisting of fluid with domain length, $L = 2m$ and width, $W = 2m$. The probe is placed at $d = 1.7m$ from the inlet. The fluid region is constrained by inviscid walls on both sides. The inflow is taken from the left and outlet is kept at the right of the fluid. The

inlet, wall, and outlet are initialized with 6 layers of particles. In order to introduce a 2D variation, the u velocity is made a function of y, given by

$$u(x, y, t) = \begin{cases} 1.0 + 0.5 \cos\left(\frac{\pi y}{12}\right) e^{\frac{(t-1)^2}{\delta}} & 1.0 < t < 1.1 \\ 1.0 & \text{elsewhere} \end{cases} . \tag{34}$$

We normalize p and u measured at the probe such that $u^* = u/u_{ref}$ and $p^* = \frac{2p}{\rho u_{ref}^2}$ respectively. Fig. 5 shows the plot of u^* and p^* versus time for the different outlets and Table 1 shows L_2 errors in the pressure and velocity for the different outlet implementations.

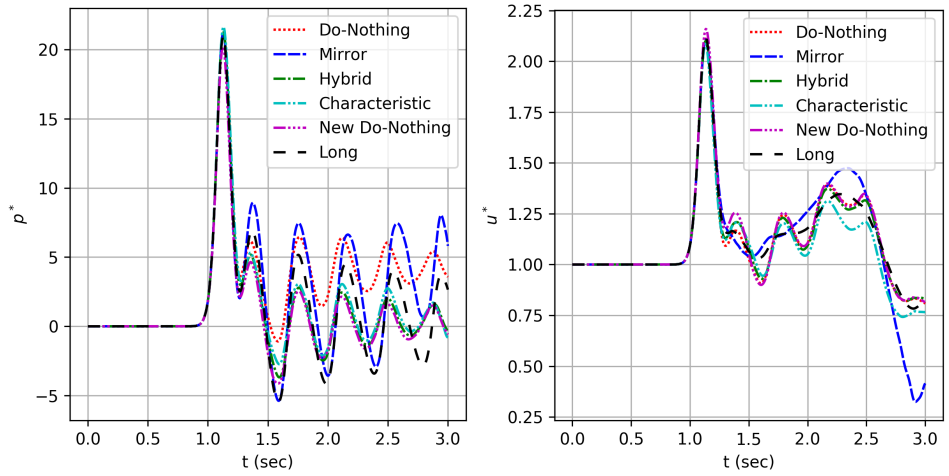


Figure 5: Normalized pressure (left) and velocity (right) plots at $x = 1.7m$ with time for 2D varying inlet.

The pressure variation with the MOC and hybrid methods are very close to the results for a long domain compared to mirroring and do-nothing outlet. It can be seen that the mirroring technique generates a lot of reflections into the fluid as compared to do-nothing and MOC. In case of the do-nothing a significant increase in pressure can be seen just after the wave passes through the outlet (at around $1.25s$).

Looking at the variation of the velocity we can see that both the modified do-nothing and the new hybrid method show a close match to the results for a long domain. After $2s$, the MOC method differs from the long-domain results due to the spatial variations arriving near the outlet. The modified do-nothing method is clearly better than the standard do-nothing scheme.

Methods	$e(p^*)$	$e(u^*)$
Characteristic	0.328	0.057
Do-Nothing	0.629	0.038
Hybrid	0.311	0.035
Mirror	0.409	0.106
New Do-Nothing	0.341	0.042

Table 1: L_2 error in the p^* and u^* measured at the probe for the 2D pulse problem.

These conclusions are also borne out by the values of the L_2 norm as seen in Table 1. The proposed hybrid method has the least errors.

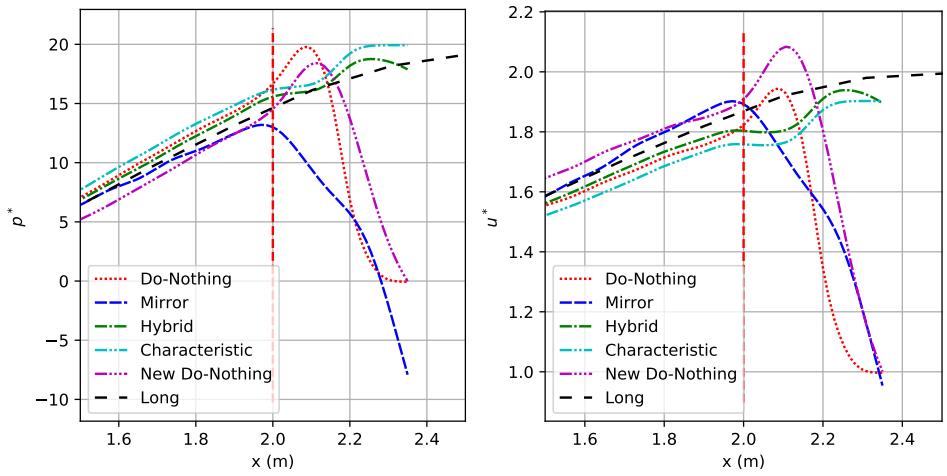


Figure 6: Normalized pressure (left) and velocity (right) along the $y = 0$ line for the 2D pulse problem. Left of the dashed red line is fluid and right is outlet region.

In order to show the nature of the property variation across the fluid outlet interface due to extrapolation, we interpolated pressure, velocity and their gradients on a $y = 0$ line as shown in Figure 6 and 7. It can be seen that, in case of the mirroring technique that the gradient of the property is zero at the interface. The property is mirrored about the domain boundary however both hybrid and do-nothing retain the history of the particle such that velocity and pressure in the outlet do not affect the upstream flow. On looking at the gradient along x of the property for all the methods in Fig.7, we find that the mirroring technique impose natural boundary conditions on fluid particles near the outlet i.e $\partial u/\partial x = 0$, and $\partial p/\partial x = 0$. In case of do-

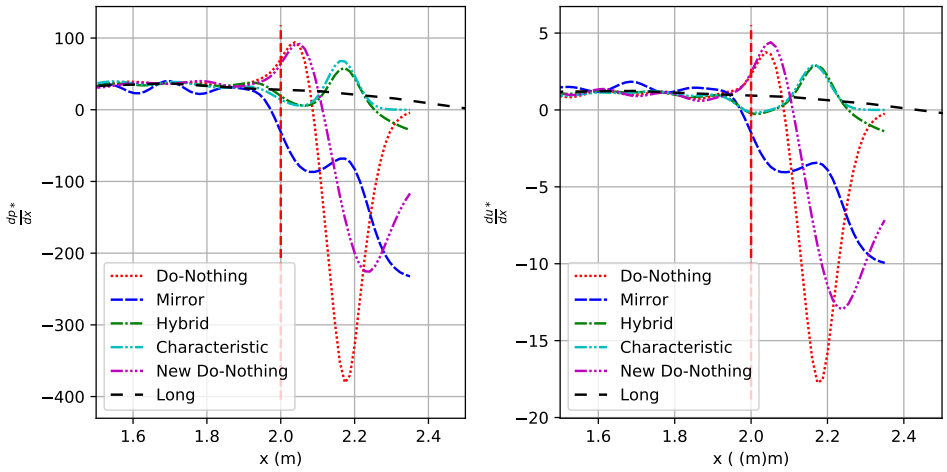


Figure 7: Normalized pressure (left) and velocity gradients (right) along the $y = 0$ line for the 2D pulse problem. Left of the dashed red line is fluid and right is outlet region.

nothing and modified do-nothing, the velocity and pressure profiles matched the long domain but gradient changes significantly. However, the method of characteristics and hybrid maintains the flow gradients along with the flow variables as they are. In the context of the SPH, the latter seems to be very important.

As discussed in section 2, the EDAC method involves a parameter called α which increases the pressure damping. We explore varying the parameter α and study the error in p^* for the different schemes in Table 2. It can be observed that as α increases the pressure oscillations are reduced and therefore the errors reduce for all the schemes. However, the greatest reduction is for the original do-nothing and mirror methods. The others are not significantly affected. This suggests that the hybrid method and modified do-nothing are robust techniques.

4.3. 1D ramp

In this test case, we impose a ramp velocity on the inlet particles such that $u = 0m/s$ at $t = 0s$ and $u = 1m/s$ at $t = 1s$. After time $t = 1s$, the velocity is fixed at $1m/s$. The size of domain, boundary condition and initialization are same as in the case of the 2D pulse. We simulate the test case for each method and compare it with results for a long domain. In the Figure 8, we have plotted the p^*, u^* for the ramp and the L_2 errors are shown in Table 3. In case of the pressure, the hybrid, mirror, and modified

Methods	$\alpha = 0.1$	$\alpha = 0.2$	$\alpha = 0.5$	$\alpha = 1.0$
Characteristic	0.336	0.334	0.328	0.315
Do-Nothing	1.135	0.864	0.629	0.587
Hybrid	0.339	0.319	0.311	0.306
Mirror	0.533	0.463	0.409	0.371
New Do-Nothing	0.391	0.543	0.341	0.354

Table 2: L_2 error in p^* measured at the probe for the 2D pulse as the EDAC parameter α.

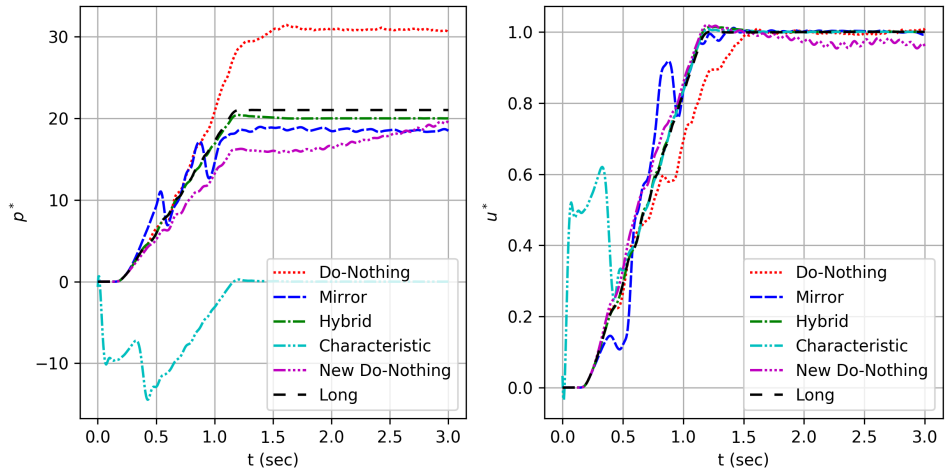


Figure 8: Normalized pressure (left) and velocity (right) plots at $x = 1.7m$ with time for ramp inlet.

do-nothing methods work well. The standard do-nothing method generates a significantly high pressure as the initial particles at the outlet do not move and thereby cause an increase in pressure. In case of the MOC, there is no specific method to determine the reference values for u, p at the initial stage and this seems to cause the problems. Similar issues are seen in the case of the velocity for the MOC. As seen in Table 3, the hybrid method has the least errors for both pressure and velocity.

4.4. 2D vortex

In this test case, a vortex is generated in the inlet moving with a constant velocity of $1m/s$ and allowed to go through the outlet. This case tests the outlet for permeability for a velocity variation similar to vortex shedding. It

Methods	$e(p^*)$	$e(u^*)$
Characteristic	1.099	0.193
Do-Nothing	0.433	0.066
Hybrid	0.043	0.007
Mirror	0.123	0.074
New Do-Nothing	0.197	0.039

Table 3: L_2 error in the p^* and u^* measured at the probe for the ramp velocity problem.

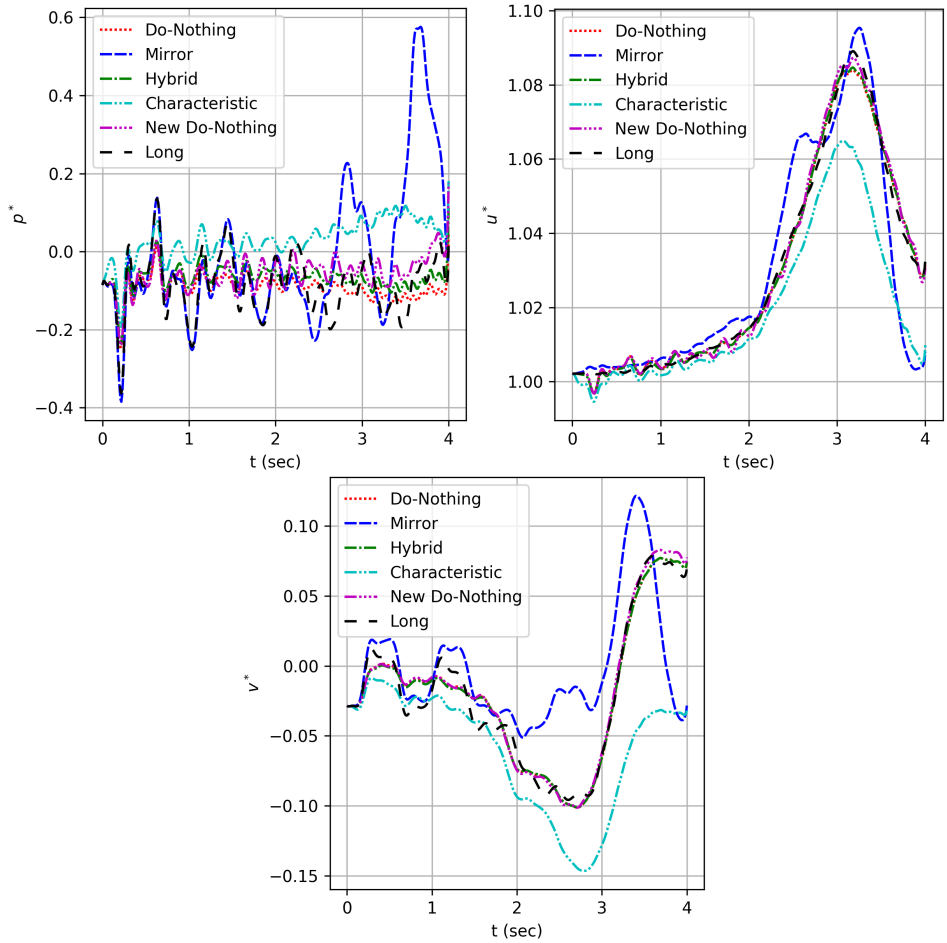


Figure 9: Normalized pressure (left), u-velocity (right) and v-velocity (center) plots at $x = 1.7m$ with time for 2D vortex advection with $1m/s$.

is important that this be preserved for most engineering flow simulations. The domain size is kept same as in case of 2D pulse however the width is doubled to accommodate the vortex. The vortex is generated by changing the velocity at the inlet with time using

$$(u, v) = \left(1.0 + \frac{\Gamma y}{r^2 + 0.2}, \frac{-\Gamma x}{r^2 + 0.2}\right), \tag{35}$$

where $\Gamma = 0.1$ is the vortex strength, and $r = \sqrt{x^2 + y^2}$ is the distance from the center of the vortex. In order to calculate the distance of the vortex we used

$$x = u(1 - t), \tag{36}$$

where u is the speed of the vortex and 1.0 is the initial distance of the vortex center from the beginning of the inlet. We test the vortex advection with the methods and compare them with the results for a long domain. In Figure 9, we have plotted the pressure and velocity for the different methods. In Table 4 the L_2 errors of the pressure and velocity are shown. It is evident from the plots that, the do-nothing, modified do-nothing, and our new hybrid method match the results of a long domain well. However, in case of mirroring technique a lot of back pressure fluctuation is visible. The MOC shows a significant deviation from the long domain and also does not preserve the velocity variation. In the pressure plot, we can see that the mirror method shows a perfect match before the vortex reaches the probe, thus it is suitable for outlets with very low gradients. However, once the vortex reaches the probe, the results of the mirror method are very poor. The L_2 errors clearly show that the do-nothing methods and the hybrid schemes work well. In particular, the error in p and v is high for the mirror and method of characteristic.

As mentioned earlier, all our simulations are inviscid which suggests an infinite Reynolds number. However, to investigate the effect of Reynolds number on the outlets we performed the above simulation at $Re = 100$ and 10000. In Table 5 and 6, we show the errors for $Re = 100$ and 10000 respectively. We can clearly see that the hybrid method and do-nothing have low errors compared other methods. We can also see that as the Reynolds number reduces and the fluid becomes increasingly viscous that the errors in the method of characteristics as well as the mirror method reduce. This clearly shows the importance of the new method.

Methods	$e(p^*)$	$e(u^*)$	$e(v^*)$
Characteristic	1.216	0.013	0.959
Do-Nothing	0.554	0.002	0.174
Hybrid	0.569	0.002	0.173
Mirror	1.588	0.010	0.806
New Do-Nothing	0.629	0.002	0.182

Table 4: L_2 error in the p^*, u^*, and v^* measured at the probe for the moving vortex problem.

Methods	$e(p^*)$	$e(u^*)$	$e(v^*)$
Characteristic	0.556	0.001	0.263
Do-Nothing	0.521	0.001	0.258
Hybrid	0.519	0.001	0.255
Mirror	0.475	0.006	0.725
New Do-Nothing	0.556	0.001	0.263

Table 5: L_2 error in the p^*, u^*, and v^* measured at the probe for the moving vortex problem, with $Re = 100$.

Methods	$e(p^*)$	$e(u^*)$	$e(v^*)$
Characteristic	1.213	0.013	0.961
Do-Nothing	0.553	0.002	0.175
Hybrid	0.566	0.002	0.173
Mirror	1.541	0.010	0.803
New Do-Nothing	0.589	0.002	0.181

Table 6: L_2 error in the p^*, u^*, and v^* measured at the probe for the moving vortex problem, with $Re = 10000$.

4.5. 2D backward-facing step

We consider the 2D backward-facing step problem. Following the experimental work of Armaly et al. [36], the step height is set as, $h = 4.9mm$ with inlet width $h_i = 5.2mm$. We compare the velocity profile at different stations with $x/h = 2.55, 3.57, 4.80, 7.14$ (where x is the distance downstream from the step). We compare our results with the experimental results in [36]. The Reynolds number of the flow is chosen to be 389 since above this the

flow is no longer two-dimensional. In the simulation, we set $\rho = 1.225kg/m^3$ and the viscosity is calculated using $Re = 2\bar{U}h/\nu$, where $\bar{U} = 2/3U_{max}$ is the mean velocity. The inlet velocity is set to $1m/s$. The schematic of the simulation model is shown below

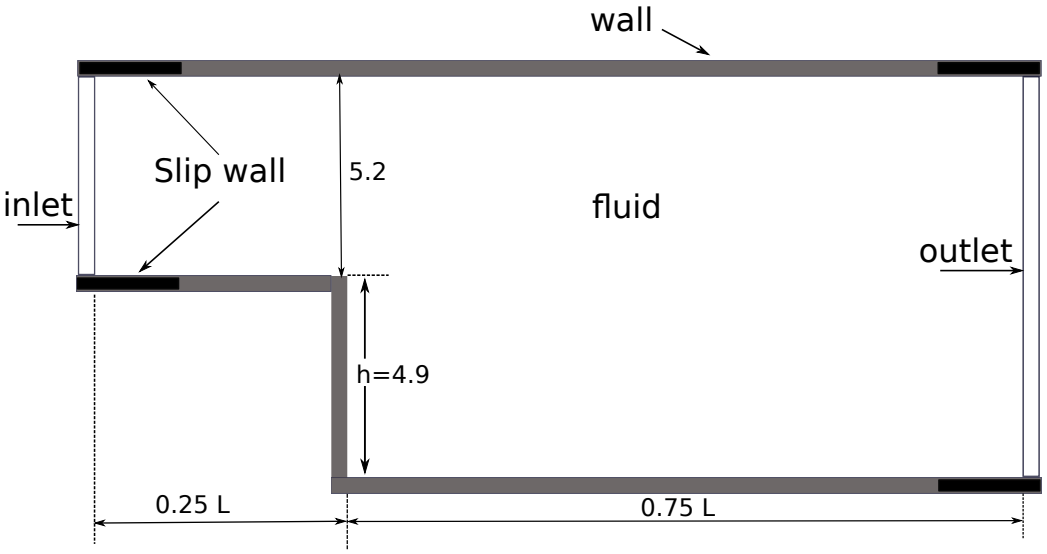


Figure 10: Sketch of domain used for backward-facing step simulations (all dimensions in mm).

At the walls, we satisfy the no-slip boundary condition. However, since the inlet is set at a constant velocity, a no-slip wall introduces non-physical pressure fluctuations. Thus a small part of the initial wall is set as a slip wall. Similarly, near the outlet we allow slip at the wall in order to avoid vortices at the start of the flow. In this test, we have shown results for our proposed method and do-nothing only, since the characteristic method and mirror methods failed to complete. In case of the mirror method, the vortices reach the outlet and the simulation blows up. In case of characteristics, the criteria for reference parameter is not known. In Figure 11, we show the velocity profile for all the methods. It is evident from the plot that all the methods (hybrid, do-nothing, and modified do-nothing) are able to reproduce the results presented by [36].

The reattachment length for the primary vortex is determined and presented in Table 7. We can clearly see that the reattachment length is very close to the experimental value 7.94 from [36]. This testcase clearly shows that the proposed method shows very less difference from the experimental

Method	x_{rl}/h
Do-Nothing	8.030
Hybrid	8.009
New Do-Nothing	7.901

Table 7: The reattachment length for $Re = 389$ for different outlet implementations.

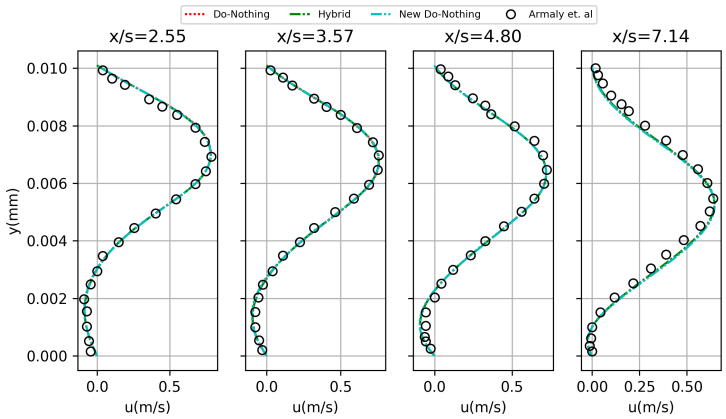


Figure 11: Velocity at $t = 1sec$ for $Re = 389$ at different locations.

values compared to other methods. This also highlights the ability of new proposed testcase to distinguish between truly non-reflecting outlet boundaries.

4.6. Flow past circular cylinder

The flow past a circular cylinder is a well known benchmark to show the capability of inlet/outlet boundaries. We investigate the problem for all the methods described in this paper. We consider a smaller domain compared to earlier research with fewer particles to show the effectiveness of the proposed method [24, 19]. A cylinder of diameter $D(= 2m)$ has been considered. The channel width is $15D$ to avoid the effect of wall and the length is $15D$, which is aligned along the x-axis. The cylinder is at $5D$ from the inlet interface as shown in Figure 12. Each inlet, outlet and wall has 6 layers of particles which are enough to get full kernel support. The inlet is given a constant prescribed velocity, $u_\infty = 1m/s$. The walls function as a slip wall in order to avoid effect of boundary layer from the walls. The fluid properties such as kinematic viscosity of the flow is evaluated using $\nu = u_\infty D/Re$, where

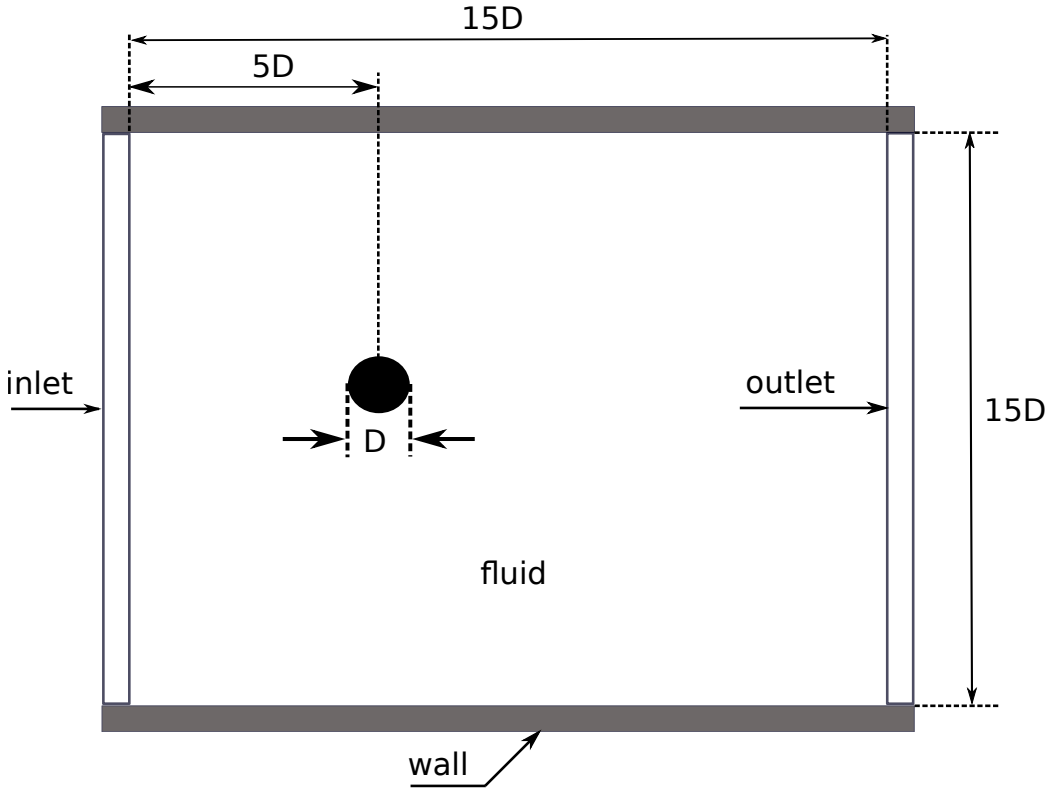


Figure 12: Sketch of domain used for flow past circular cylinder simulations.

Re is the Reynolds number of the flow and density $\rho = 1000kg/m^3$. We use a particle spacing $\Delta x = 0.0667$ and $h/\Delta x = 1.2$ which result in 201694 fluid particles in the domain. This spacing results in a cell Reynolds number of $Re_{cell} = u_\infty h/\nu$ of 8. This suggests that this is a coarse simulation. In order to capture the curvature of the cylinder, we place the particles in the solid such that the volume is consistent. We first place particles on the circumference spaced Δx from each other and then create points on a circle Δx towards center and perform the same procedure until we reach the center.

We simulate the model for $Re = 200$ for all the methods. In the Fig. 13 and 14 we have plotted p^* and u^* respectively at $t = 50s$ for all methods. Since the gradient near the outlet boundary is close to zero, all the methods show similar variations. However after vortex shedding starts, the gradient near the outlet is large. In Fig. 15 and 16 we show the pressure and velocity distribution at $t = 150s$ respectively, when the vortex shedding is well

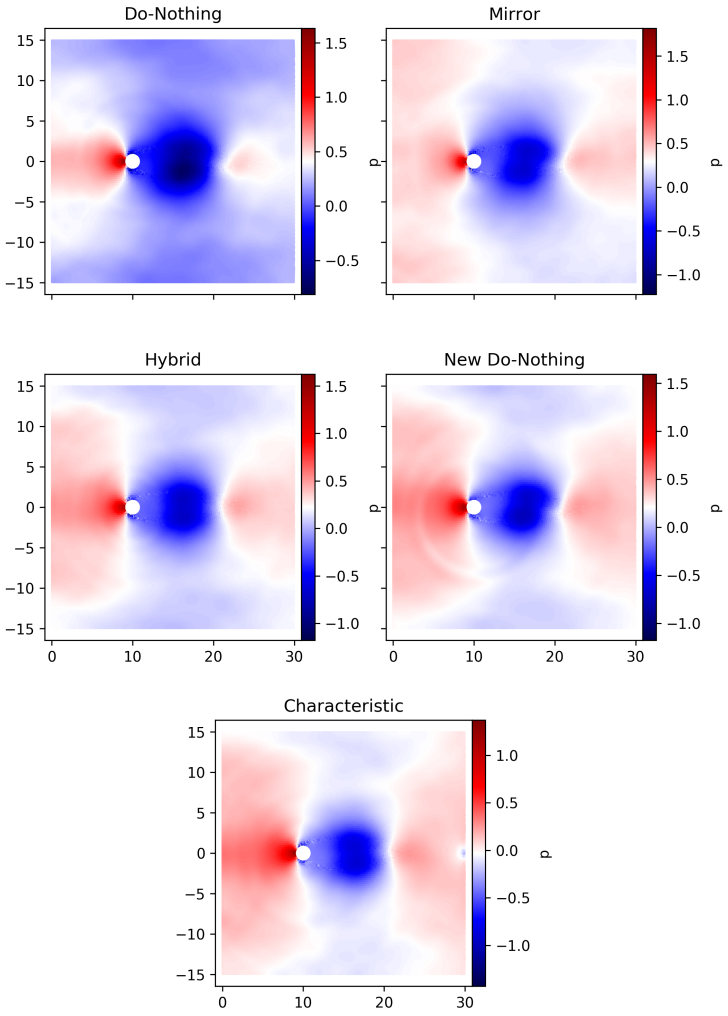


Figure 13: Normalized pressure at $t = 50sec$ for $Re = 200$.

established. In case of mirror method due to high gradient near the outlet, spurious pressures arise and the particle positions diverge. It is evident from

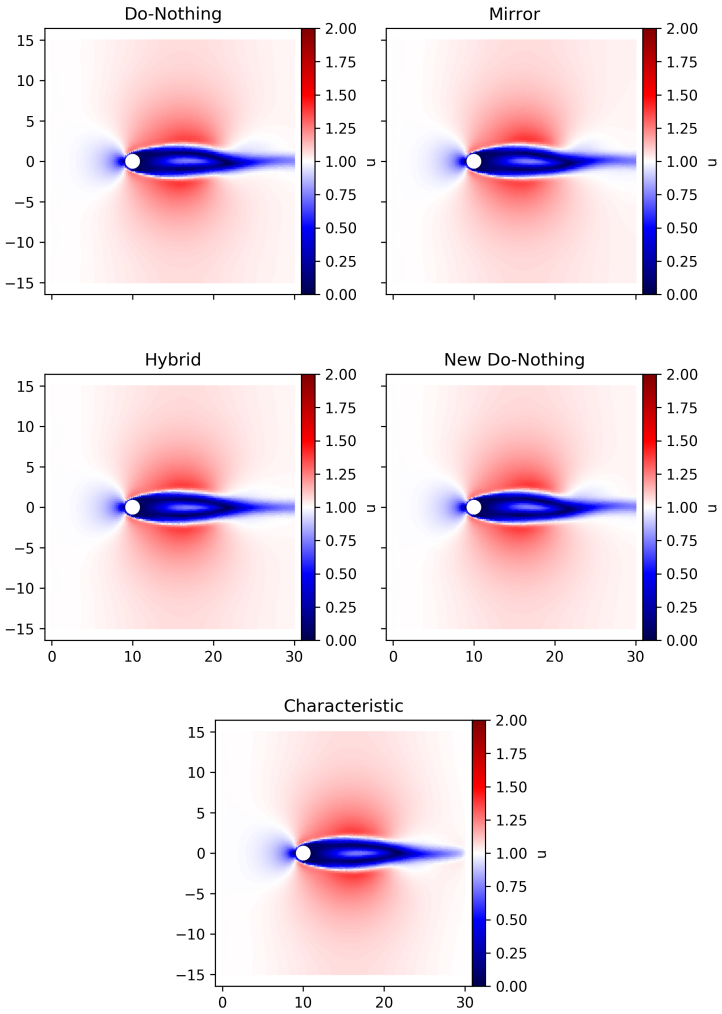


Figure 14: Normalized velocity at $t = 50sec$ for $Re = 200$.

the pressure plots in Fig. 15 that the MOC reflects the pressure back into the domain when vortex shedding starts. In case of do-nothing and modified do-

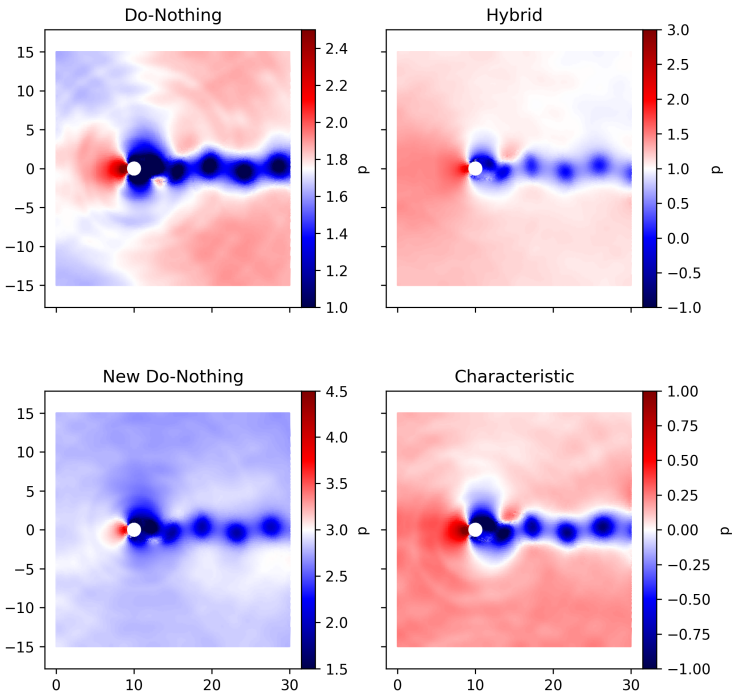


Figure 15: Normalized pressure at $t = 150sec$ for $Re = 200$.

nothing a significant increase in pressure of the domain is visible. Pressure for both hybrid and characteristic method looks to be distributed around zero which is essential for low numerical errors in pressure calculations. In Fig. 16 of velocity distributions, all the methods show a similar pattern and it is hard to comment on the relative merits of the methods.

In order to check the accuracy of the methods, we calculate the drag ($F_d = F_x$) and lift ($F_l = F_y$) forces on the cylinder for all the cases and evaluate the coefficient of drag, $c_d = F_d/(0.5\rho u_\infty^2)$, and lift $c_l = F_l/(0.5\rho u_\infty^2)$. A five point average is taken to filter the noise. The force on the solid cylinder is determined by solving the momentum equation given by

$$\frac{F_{solid}}{m_{solid}} = -\frac{1}{\rho}\nabla p + \nu\nabla^2\mathbf{u}. \tag{37}$$

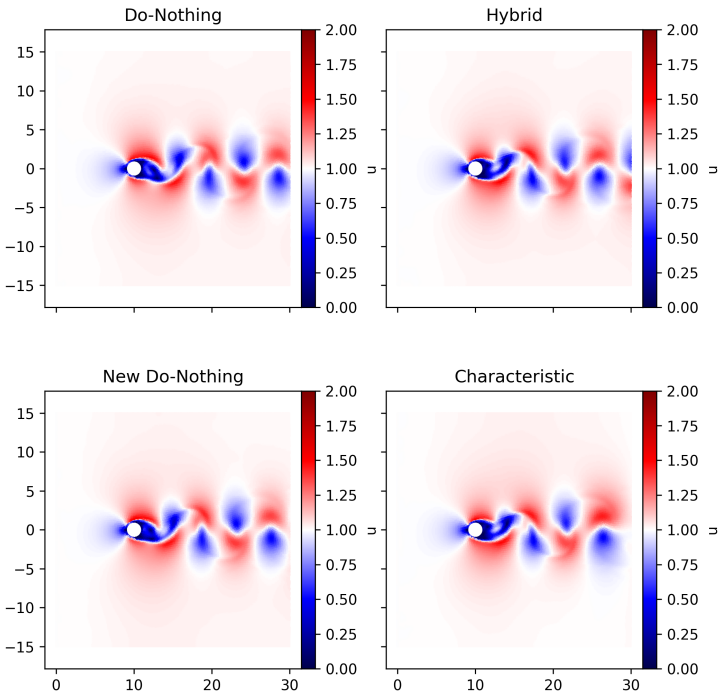


Figure 16: Normalized velocity at $t = 150sec$ for $Re = 200$.

The above equation in the SPH form is given by

$$F_{solid} = \sum_j \left(V_i^2 + V_j^2\right) \left[-\tilde{p}_{ij}\nabla W_{ij} + \tilde{\eta}_{ij}\frac{\mathbf{u}_{ij}}{(r_{ij}^2 + \eta h_{ij}^2)}\nabla W_{ij} \cdot \mathbf{r}_{ij}\right], \tag{38}$$

where all symbols have same meaning as given in section 2 except $u_{ij} = u_{g_i} - u_j$, where u_{g_i} is the solid wall velocity [6]. We also evaluate the Strouhal number $St = fD/u_\infty$ where f is the frequency of shedding. In Fig. 17, we compare c_l for all the methods over time. It can be easily seen that mirror method blows up after a large back pressure. In case of do-nothing and modified do-nothing, shedding starts earlier compared to hybrid and characteristic method. In Table 8, we compare c_d and c_l and St for all the methods and with results published by [37, 19, 24]. We can see that in spite of having non-physical pressure variations in characteristic methods the value

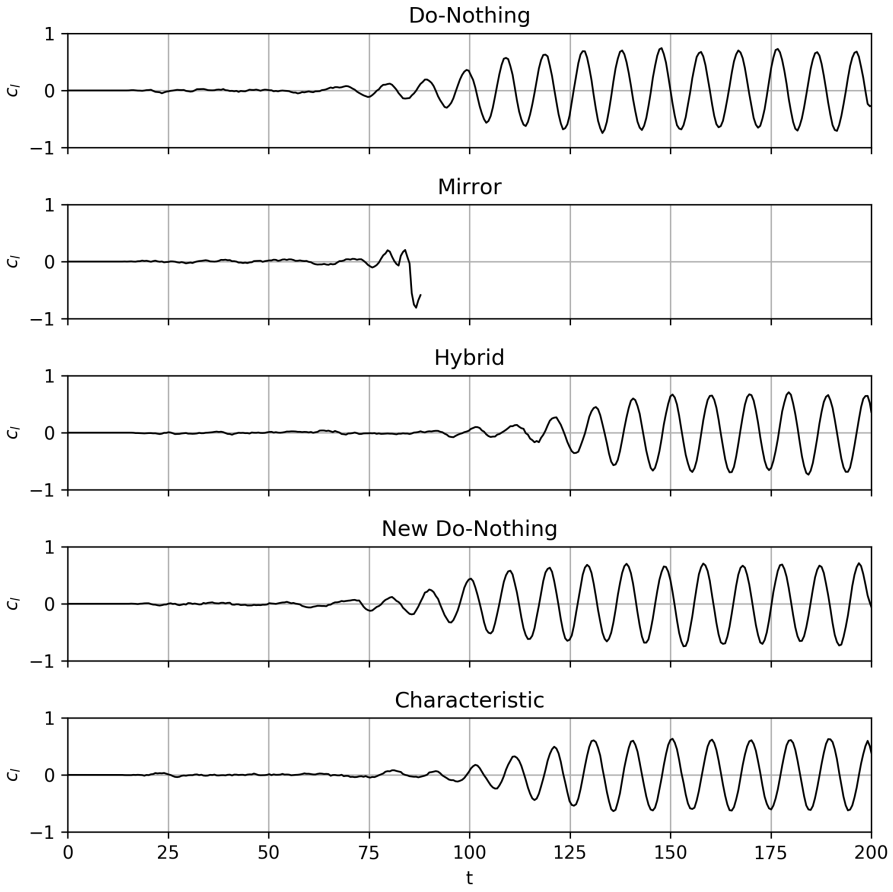


Figure 17: Plot for c_d for all methods at Re=200

of c_d and c_l shows a close match. In case of both do-nothing and modified do-nothing the values are close since the pressure increase of the domain is insignificant in case of incompressible flows. In our proposed hybrid method, the pressure and velocity plots looks similar to [24, 19], the c_d and c_l are in acceptable range presented in literature. Furthermore, the proposed hybrid and modified do-nothing methods have been tested for Reynolds number 20. In the Fig. 18, we show the c_d and c_l for hybrid and modified do-nothing. It is evident from the figure that both modified do-nothing and hybrid produces

Method	c_d	c_l	St
Characteristic	1.494 ± 0.05	± 0.634	± 0.200
Do-Nothing	1.532 ± 0.05	± 0.744	± 0.210
Hybrid	1.524 ± 0.05	± 0.722	± 0.210
New Do-Nothing	1.540 ± 0.05	± 0.729	± 0.210
Marrone et al. [19]	1.38 ± 0.05	± 0.680	0.200
Guerrero [37]	1.409 ± 0.048	± 0.725	-
Tafuni et al. [24]	1.46	± 0.693	0.206

Table 8: Comparison of c_l, c_d and St values for different method with literature for $Re = 200$.

Particle Spacing	Hybrid	New do-nothing
0.05	2.317	2.317
0.07	2.320	2.321
0.10	2.317	2.319

Table 9: Convergence of c_d with the decrease in particle spacing at Re=20 for hybrid method

similar results. However hybrid is better than the modified do-nothing as shown in other test cases. In order to check the convergence of the results, we perform a convergence study for both the proposed methods and tabulated the results in Table 9 at $Re = 20$. We observe that c_d decreases with decrease in particle spacing and converges to around 2.317. When the spacing is 0.05 the cell Reynolds number is 0.6 suggesting a sufficiently resolved simulation. It must be noted that the results presented are in a smaller domain and with much fewer particles than those used in earlier research which show that the proposed methods replace need of a large domain for wind-tunnel type of simulations. The results above also show that the flow past a circular cylinder does not reveal important differences between the different boundary conditions and the importance of our proposed test problems.

5. Conclusions

In this paper we review the established techniques for implementing outlet boundaries in the context of weakly-compressible SPH schemes. We classify

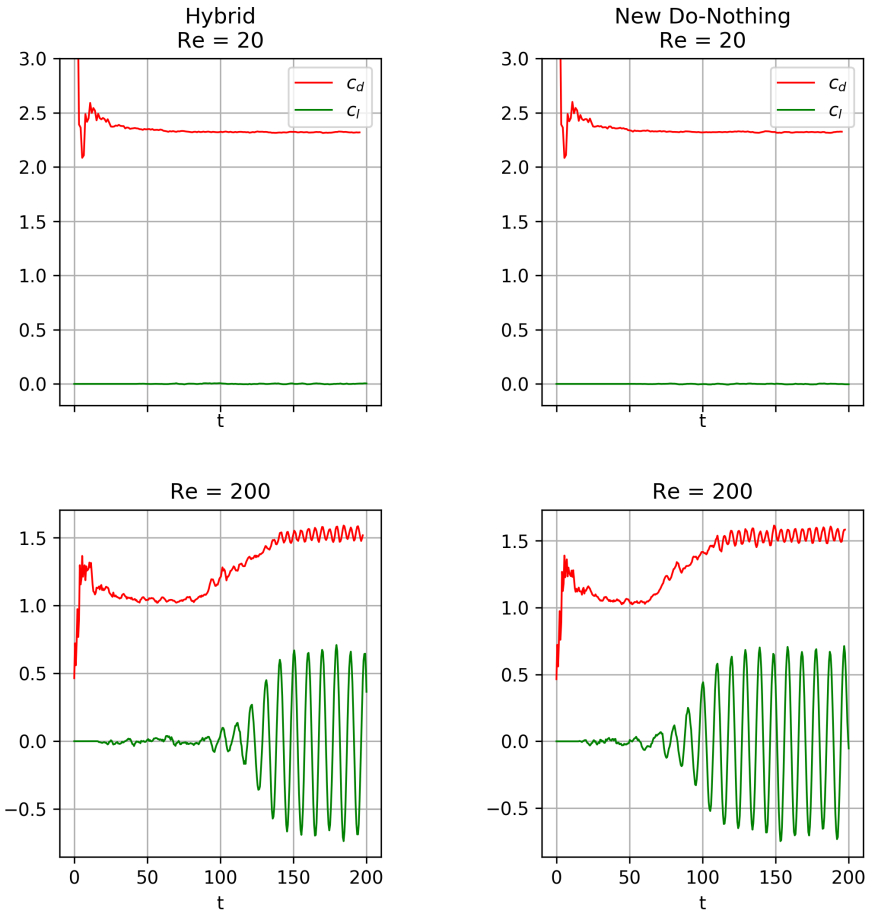


Figure 18: Plot for c_d and c_l for hybrid and the modified do-nothing at Re=20 and 200.

them into three broad categories. In order to systematically examine these, we construct four simple test problems. These tests clearly show the deficiencies of the existing approaches.

- Do-nothing method is only suitable for problems where high intensity acoustic pressure waves are absent.
- The mirror method works best for flows where the gradients are very low near the outlet.

- The MOC show excellent results where reference properties are known a priori but are not very effective when there are gradients in the flow at the exit.

Based on this, we propose a new generalized scheme which combines the do-nothing and characteristic based outlet into a new hybrid technique. The proposed technique works well with both high intensity acoustic waves and high gradient flow near the outlet. Unlike the MOC, it calculates reference flow variables by time averaging. We also propose a much simpler and slightly modified do-nothing boundary condition that produces good results. We then demonstrate these with simulations of the flow past a circular cylinder at two different Reynolds numbers and also for the flow past a backward-facing step. We are able to obtain very good results with much fewer particles than reported earlier. Finally, our implementation is open source and our manuscript is fully reproducible.

Acknowledgements

The authors are grateful to Prof. Krishnendu Haldar of the Department of Aerospace Engineering, IIT Bombay for providing us with his workstation to expedite our simulations.

References

References

1. Gingold, R.A., Monaghan, J.J.. Smoothed particle hydrodynamics: Theory and application to non-spherical stars. *Monthly Notices of the Royal Astronomical Society* 1977;181:375–389.

2. Lucy, L.B.. A numerical approach to testing the fission hypothesis. *The Astronomical Journal* 1977;82(12):1013–1024.

3. Monaghan, J.J.. Smoothed Particle Hydrodynamics. *Reports on Progress in Physics* 2005;68:1703–1759.

4. Monaghan, J.J.. Simulating free surface flows with SPH. *Journal of Computational Physics* 1994;110:399–406.

5. Adami, S., Hu, X., Adams, N.. A transport-velocity formulation for smoothed particle hydrodynamics. *Journal of Computational Physics* 2013;241:292–307. URL: http://linkinghub.elsevier.com/retrieve/pii/S002199911300096X. doi:10.1016/j.jcp.2013.01.043.

6. Zhang, C., Hu, X.Y.T., Adams, N.A.. A generalized transport-velocity formulation for smoothed particle hydrodynamics. *Journal of Computational Physics* 2017;337:216–232.

7. Lind, S., Xu, R., Stansby, P., Rogers, B.. Incompressible smoothed particle hydrodynamics for free-surface flows: A generalised diffusion-based algorithm for stability and validations for impulsive flows and propagating waves. *Journal of Computational Physics* 2012;231(4):1499 – 1523. doi:10.1016/j.jcp.2011.10.027.

8. Skillen, A., Lind, S., Stansby, P.K., Rogers, B.D.. Incompressible smoothed particle hydrodynamics (SPH) with reduced temporal noise and generalised fickian smoothing applied to body–water slam and efficient wave–body interaction. *Computer Methods in Applied Mechanics and Engineering* 2013;265:163 – 173. doi:10.1016/j.cma.2013.05.017.

9. Gomez-Gesteria, M., Rogers, B.D., Dalrymple, R.A., Crespo, A.J.. State-of-the-art classical SPH for free-surface flows. *Journal of Hydraulic Research* 2010;84:6–27.

10. Antuono, M., Colagrossi, A., Marrone, S., Molteni, D.. Free-surface flows solved by means of SPH schemes with numerical diffusive terms. *Computer Physics Communications* 2010;181(3):532 – 549. doi:https://doi.org/10.1016/j.cpc.2009.11.002.

11. Ramachandran, P., Puri, K.. Entropically damped artificial compressibility for SPH. *Computers and Fluids* 2019;179(30):579–594. doi:10.1016/j.compfluid.2018.11.023.

12. Cummins, S.J., Rudman, M.. An SPH projection method. *Journal of Computational Physics* 1999;152:584–607.

13. Shao, S., Lo, E.Y.. Incompressible SPH method for simulating newtonian and non-newtonian flows with a free surface. *Advances*

in Water Resources 2003;26(7):787 – 800. URL: http://www.sciencedirect.com/science/article/pii/S0309170803000307. doi:https://doi.org/10.1016/S0309-1708(03)00030-7.

14. Hu, X., Adams, N.. An incompressible multi-phase SPH method. *Journal of Computational Physics* 2007;227(1):264–278. URL: http://linkinghub.elsevier.com/retrieve/pii/S0021999107003300. doi:10.1016/j.jcp.2007.07.013.

15. Lastiwka, M., Basa, M., Quinlan, N.J.. Permeable and non-reflecting boundary conditions in SPH. *International Journal for Numerical Methods in Fluids* 2009;61(7):709–724. URL: https://onlinelibrary.wiley.com/doi/abs/10.1002/fld.1971. doi:10.1002/fld.1971.

16. Liu, W.K., Jun, S., Zhang, Y.F.. Reproducing kernel particle methods. *International Journal for Numerical Methods in Fluids* 1995;20(8-9). URL: http://dx.doi.org/10.1002/fld.1650200824. doi:10.1002/fld.1650200824.

17. Bonet, J., Lok, T.S.. Variational and momentum preservation aspects of smooth particle hydrodynamic formulations. *Computer Methods in Applied Mechanics and Engineering* 1999;180(1):97 – 115. URL: http://www.sciencedirect.com/science/article/pii/S0045782599000511. doi:10.1016/S0045-7825(99)00051-1.

18. Federico, I., Marrone, S., Colagrossi, A., Aristodemo, F., Antuono, M.. Simulating 2D open-channel flows through an SPH model. *European Journal of Mechanics - B/Fluids* 2012;34:35 – 46. URL: http://www.sciencedirect.com/science/article/pii/S0997754612000337. doi:https://doi.org/10.1016/j.euromechflu.2012.02.002.

19. Marrone, S., Colagrossi, A., Antuono, M., Colicchio, G., Graziani, G.. An accurate SPH modeling of viscous flows around bodies at low and moderate reynolds numbers. *Journal of Computational Physics* 2013;245:456 – 475. URL: http://www.sciencedirect.com/science/article/pii/S0021999113001885. doi:https://doi.org/10.1016/j.jcp.2013.03.011.

20. Molteni, D., Grammauta, R., Vitanza, E.. Simple absorbing layer conditions for shallow wave simulations with smoothed particle hydrodynamics. *Ocean Engineering* 2013;62:78 – 90. URL: http://www.sciencedirect.com/science/article/pii/S0029801813000097. doi:https://doi.org/10.1016/j.oceaneng.2012.12.048.

21. Khorasanizade, S., Sousa, J.M.M.. An innovative open boundary treatment for incompressible sph. *International Journal for Numerical Methods in Fluids* 2015;80(3):161–180. URL: https://onlinelibrary.wiley.com/doi/abs/10.1002/fld.4074. doi:10.1002/fld.4074.

22. Alvarado-Rodríguez, C.E., Klapp, J., Sigalotti, L.D.G., Domínguez, J.M., de la Cruz Sánchez, E.. Nonreflecting outlet boundary conditions for incompressible flows using SPH. *Computers & Fluids* 2017;159:177 – 188. URL: http://www.sciencedirect.com/science/article/pii/S0045793017303559. doi:https://doi.org/10.1016/j.compfluid.2017.09.020.

23. Jin, G., Braza, M.. A nonreflecting outlet boundary condition for incompressible unsteady navier-stokes calculations. *Journal of Computational Physics* 1993;107(2):239 – 253. URL: http://www.sciencedirect.com/science/article/pii/S002199918371140X. doi:https://doi.org/10.1006/jcph.1993.1140.

24. Tafuni, A., Domínguez, J., Vacondio, R., Crespo, A.J.C.. A versatile algorithm for the treatment of of open boundary conditions in smoothed particle hydrodynamics GPU models. *Computer methods in applied mechanical engineering* 2018;342:604–624. doi:10.1016/j.cma.2018.08.004.

25. Liu, M., Liu, G.. Restoring particle consistency in smoothed particle hydrodynamics. *Applied Numerical Mathematics* 2006;56(1):19 – 36. URL: http://www.sciencedirect.com/science/article/pii/S0168927405000565. doi:https://doi.org/10.1016/j.apnum.2005.02.012.

26. Wang, P., Zhang, A.M., Ming, F., Sun, P., Cheng, H.. A novel nonreflecting boundary condition for fluid dynamics solved by smoothed

particle hydrodynamics. *Journal of Fluid Mechanics* 2019;860:81–114. doi:10.1017/jfm.2018.852.

27. Hosseini, S.M., Feng, J.J.. Pressure boundary conditions for computing incompressible flows with SPH. *Journal of Computational Physics* 2011;230(19):7473 – 7487. URL: http://www.sciencedirect.com/science/article/pii/S0021999111003779. doi:https://doi.org/10.1016/j.jcp.2011.06.013.

28. Pahar, G., Dhar, A.. Robust boundary treatment for open-channel flows in divergence-free incompressible SPH. *Journal of Hydrology* 2017;546:464 – 475. doi:https://doi.org/10.1016/j.jhydrol.2017.01.034.

29. Monteleone, A., Monteforte, M., Napoli, E.. Inflow/outflow pressure boundary conditions for smoothed particle hydrodynamics simulations of incompressible flows. *Computers & Fluids* 2017;159:9 – 22. URL: http://www.sciencedirect.com/science/article/pii/S0045793017303468. doi:https://doi.org/10.1016/j.compfluid.2017.09.011.

30. Ramachandran, P.. PySPH: a reproducible and high-performance framework for smoothed particle hydrodynamics. In: Benthall, S., Rostrup, S., eds. *Proceedings of the 15th Python in Science Conference*. 2016:127 – 135. doi:10.25080/Majora-629e541a-011.

31. Ramachandran, P., Puri, K., et al. PySPH: a python-based SPH framework. 2010–. URL: http://pypi.python.org/pypi/PySPH/.

32. Ramachandran, P.. automan: A python-based automation framework for numerical computing. *Computing in Science & Engineering* 2018;20(5):81–97. URL: doi.ieeecomputersociety.org/10.1109/MCSE.2018.05329818. doi:10.1109/MCSE.2018.05329818.

33. Adami, S., Hu, X., Adams, N.. A generalized wall boundary condition for smoothed particle hydrodynamics. *Journal of Computational Physics* 2012;231(21):7057–7075. URL: http://linkinghub.elsevier.com/retrieve/pii/S002199911200229X. doi:10.1016/j.jcp.2012.05.005.

34. Giles, M.B.. Nonreflecting boundary conditions for Euler equation calculations. *AIAA Journal* 1990;28(12):2050–2058.

35. Kinsler, L.E., Frey, A.R., Coppens, A.B., Sanders, J.V.. Fundamentals of acoustics. *Fundamentals of Acoustics, 4th Edition, by Lawrence E Kinsler, Austin R Frey, Alan B Coppens, James V Sanders, pp 560 ISBN 0-471-84789-5 Wiley-VCH, December 1999* 1999;:560.

36. Armaly, B., J. Durst, F., Pereira, J., Schönung, B.. Experimental and theoretical investigation of backward-facing step flow. *Journal of Fluid Mechanics* 1983;127:473 – 496. doi:10.1017/S0022112083002839.

37. Guerrero, J.. Numerical simulation of the unsteady aerodynamics of flapping flight. *Department of Civil, Environmental, Architectural Engineering* 2009;.